CHAPTER 4

Multipoint Correlation Functions for Photon Statistics in Single-Molecule Spectroscopy: Stochastic Dynamics in Liouville Space

František Šanda* and Shaul Mukamel†

*Charles University, Faculty of Mathematics and Physics, Institute of Physics, Ke Karlovu 5, Prague, 121 16 Czech Republic
†Department of Chemistry, University of California, Irvine, CA 92697-2025

1. Photon statistics: Factorial moments vs. correlation functions

Single-molecule spectroscopy (SMS) had opened up new windows into the molecular world by providing a wealth of information about fluctuations of elementary molecular events.[1–4] SMS directly measures statistical distributions of various properties and observes the spectroscopic trace of slowly varying (~msec) parameter trajectories. Photon arrival trajectories obtained in response to a train of excitation pulses were employed to extract similar information for faster (~nsec) environmental changes on the radiative lifetime timescale, where the statistical properties of parametric fluctuations affect the photon emission.[5,6] Statistical analysis of SMS signals is usually

based on two-point distributions or correlation functions. Higher statistical measures provide independent additional information when the dynamics is nonMarkovian and may not be completely described in terms of two-point Green functions. For example, two-point measures of the fluorescence trace only provide partial information about the underlying internal dynamics, which is usually not sufficient to establish Markovian description of all the relevant degrees of freedom. Multipoint quantities may be instrumental for distinguishing among various possible models.[7–13] Formal analogy between some SMS observables and coherent nonlinear signals[14] will be discussed.

We shall consider two elementary observables in continuous wave (cw) experiments: the number of photons $N(\tau)$ detected during a binning time τ, and the photon emission intensity $I(\tau)$. The two are connected by

$$I(\tau) \equiv \frac{N(\tau + \Delta\tau) - N(\tau)}{\Delta\tau}, \quad \Delta\tau \to 0. \tag{1}$$

The k-point correlation function $g^{(k)}$ of fluorescence intensities I is defined by

$$g^{(k)}(t_{k-1}, \ldots, t_1) \equiv \langle I(t_{k-1} + \cdots + t_1) \cdots I(t_1) I(0) \rangle \tag{2}$$

or in a normalized form,

$$h^{(k)}(t_{k-1}, \ldots, t_1) \equiv \frac{\langle I(t_{k-1} + \cdots + t_1) \cdots I(t_1) I(0) \rangle}{\langle I(t_{k-1} + \cdots + t_1) \rangle \cdots \langle I(t_1) \rangle \langle I(0) \rangle}, \tag{3}$$

where $t_j = \tau_j - \tau_{j-1}$ are the intervals between the observation times τ_j. We have set $\tau_0 = 0$ so that $\tau_j = t_j + \cdots + t_1$.

Photon counting distributions may be characterized by the kth factorial moments $F^{(k)}(\tau) \equiv \langle N(N-1) \cdots (N-k+1) \rangle$. Single photon

emission is a stochastic event, whose most basic characteristics are its mean and variance. The latter is traditionally expressed in terms of the Mandel parameter

$$M(\tau) \equiv \frac{\langle N(N-1) \rangle - \langle N \rangle^2}{\langle N \rangle}. \tag{4}$$

For Poissonian statistics (independent emission events) we have $M = 0$. Sub-Poissonian $M < 0$ (superPoissonian $M > 0$) statistics shows up as photon antibuching (bunching). For long binning times we expect the distributions of N to approach a Gaussian form, in agreement with the central limit theorem. Some exceptions are the photon distributions of anomalously relaxing systems.[15,16] Such nonergodic systems do not equilibrate and their Mandel parameter grows asymptotically linearly with time[17,18] instead of approaching a limiting value as expected for normal relaxation.[19,20]

A few assumptions are inherent in the modeling of photon counting experiments. The precise emission time is assumed to be sharp, and any coherence between the initial and the final states of the emission process is neglected. The photon emission is then described by a quantum master equation (QME)[21,22]:

$$\left(\frac{d\rho}{dt}\right)_M = \frac{1}{2} \sum_{i>j} \Gamma_{i\to j} (-S_{ij}^\dagger S_{ij} \rho + 2 S_{ij} \rho S_{ij}^\dagger - \rho S_{ij}^\dagger S_{ij}), \tag{5}$$

where ρ is the molecular density matrix, $S_{ij}^\dagger \equiv |i\rangle\langle j|$ ($S_{ij} \equiv |j\rangle\langle i|$) are raising (lowering) operators connected with the radiative transition from level $|i\rangle$ to a lower level $|j\rangle$, and $\Gamma_{i\to j}$ are the corresponding spontaneous emission rates. Equation (5) may be derived microscopically starting with the quantum Hamiltonian of the radiation field by assuming that the molecular levels are well separated so that coherences may be neglected,[20] i.e. each photon can be associated with a distinct transition between a specific pair of levels. Equation (5) can be generalized to account for cooperative emission.[22,23]

The QME provides a classical trajectory picture for the quantum dynamics of the radiation field. The emission event can be analyzed in classical terms, since observing a photon with a given frequency uniquely defines the state of the system after that event. The same can be said about a quantum measurement. In fact, photon emission is a kind of quantum measurement. It is different from the standard von Neumann measurements[24] since the effect on the molecular wavefunction is not described by a simple projection operator, as the emission is necessarily accompanied by an annihilation of excitation. However, as in the von Neumann measurement, the emission event erases coherences through a "quantum collapse" and defines the future state of the system by providing a statistical prediction as to which photons will be subsequently observed and when.

Single-molecule experiments directly provide time-averaged correlation functions. However, most theoretical approaches focus on ensemble averages, and use the ergodic hypothesis to predict time-averaged observables. Nonergodic, anomalously relaxing, single molecules do not explore the state space uniformly,[17,25] and a description in terms of distributions of time averages is then necessary.[26]

The factorial moments are also introduced for nontrivial time-dependent driving, e.g., to test the quality of single-photon sources, and optimize a given number of emitted photons by manipulating the laser source.[27,28] In these cases the statistical distributions of the emitted photons are more suitable than multipoint correlation functions. For spectroscopic measurements on stationary samples the information content of both measures is similar, as will be shown below.

SMS supplements bulk measurements of biomolecules, quantum dots, and aggregates.[29,30] We assume a stationary cw experiment and the ergodic hypothesis to hold. As a consequence of Eq. (5) the time evolution is not described by a unitary transformation in Hilbert space, and a Liouville space description is preferable.[14,31] We shall adopt tetradic Liouville-space notation. The elements of Liouville space are $|jk\rangle\rangle \equiv |j\rangle\langle k|$. Molecular density ρ, which is a matrix in

Eq. (5) now becomes a vector in this higher space. For instance, Eq. (5) reads

$$\left(\frac{d\rho}{dt}\right)_M = \frac{1}{2}\sum_{i>j}\Gamma_{i\to j}\left(-S_{ij}^{\dagger(L)}S_{ij}^{(L)}\rho + 2S_{ij}^{(L)}S_{ij}^{\dagger(R)}\rho - S_{ij}^{(R)}S_{ij}^{\dagger(R)}\rho\right), \tag{6}$$

where the left (right) superoperators are defined by their action on Hilbert space operator (Liouville space element) X; $A^{(L)}X \equiv AX$ ($A^{(R)}X \equiv XA$). Using this notation we can describe the photon emission by the resetting superoperator R, defined by the positive contributions to the right-hand side of Eq. (5)[32]:

$$R \equiv \sum_{i>j}\Gamma_{i\to j}S_{ij}^{(L)}S_{ij}^{\dagger(R)} = \sum_{i>j}|jj\rangle\rangle\Gamma_{i\to j}\langle\langle ii|. \tag{7}$$

The resetting superoperator R connects the density matrix before and after emission events.

The full dynamics of the system is described by Liouville equation:

$$\frac{d\rho}{dt} = \mathcal{L}\rho + E(t)\mathcal{L}_{\text{int}}\rho + \left(\frac{d\rho}{dt}\right)_M, \tag{8}$$

where $\mathcal{L}_{\text{int}} = (-i/\hbar)[H_{\text{int}}, \ldots]$ describe the interaction with a classical electric field and $\mathcal{L}$ describe the internal dynamics of the system (including a bath), which need not be necessarily induced by Hamiltonian description (e.g., the stochastic Liouville equations).

The superoperator Green function solution $\mathcal{G}(t)$ to Eq. (8) represents the evolution of the optically driven system in Liouville space between emission events. Hereafter in this section we treat all relevant degrees of freedom explicitly so that $\mathcal{G}(t)$ represents a Markovian evolution in that space, and with the rotating wave approximation it only depends on differences between the two times (see Ref. 20). The complete distribution of photons may be conveniently calculated using the generating function technique[33–36] which is explained in

Chap. 3 of this book. The multipoint correlation function (2) can be calculated by[20]

$$g^{(k)}(t_{k-1},\ldots,t_1) = \mathrm{Tr}[R\mathcal{G}(t_{k-1})R\cdots\mathcal{G}(t_1)R\rho_s], \tag{9}$$

where ρ_s is the steady-state density matrix. The Laplace domain expression ($\mathcal{G}(s) \equiv \int_0^\infty e^{-st}\mathcal{G}(t)dt$) for the kth factorial moment is (Eqs. (C1)–(C5) in Ref. 20)

$$F^{(k)}(s) = k!\frac{1}{s^2}\mathrm{Tr}(R\mathcal{G}(s))^{k-1}R\rho_s. \tag{10}$$

Prefactor $\frac{1}{s^2}$ corresponds to double integration in time domain; and by comparing Eq. (10) with the Laplace transform of Eq. (11) we see that the two quantities are connected by

$$F^{(k)}(t) = k!\int_0^t d\tau' \int_0^{\tau'} d\tau_{k-1}\int_0^{\tau_{k-1}} d\tau_{k-2}\ldots \times \int_0^{\tau_2} d\tau_1 g^{(k)}(\tau_{k-1}-\tau_{k-2},\ldots,\tau_1-\tau_0) \tag{11}$$

The lowest $k = 1$ and 2 moments and correlation functions carry identical information and we have

$$N(t) = t\langle I\rangle,$$

where $\langle I\rangle \equiv g^{(1)}$ and

$$M(t) = \frac{2\langle I\rangle}{t}\int_0^t dt' \int_0^{t'} dt_1[h^{(2)}(t_1)-1]$$
$$h^{(2)}(t) = 1 + (2\langle I\rangle)^{-1}\frac{d^2}{dt^2}tM(t). \tag{12}$$

For $k > 2$, Eq. (11) may not be inverted, since $g^{(k)}$ carry more information than $F^{(k)}$; obviously, one cannot derive the $(k-1)$-parameter multipoint correlation function from the one-parameter factorial moment.

2. Photon statistics in weakly driven systems: Analogy with four wave mixing

We first discuss the basic phenomenology of SMS using a single two-level model system (TLS). The resetting is a nonequilibrium operation and photon counting carries a different information in single molecule and in bulk experiments. Consider the probability $g^{(2)}(t_1)$ to observe two photon emissions at times 0 and t_1. Immediately following an emission event, the steady state is perturbed: The TLS is in the ground state and it cannot emit another photon so that $h^{(2)}(0) = 0$. A single two-level chromophore cannot emit twice in a short time interval. This effect is known as antibunching. In bulk measurements the other molecules may still emit,[37] and antibunching is suppressed since the correlation function $h_V^{(2)}$ for V independent identical chromophores

$$h_V^{(2)} = 1 + \frac{1}{V}(h_1^{(2)} - 1)$$

approaches 1 for $V \to \infty$. Antibunching persists for shorter times than the ground state recovery time, which for a weakly driven TLS coincides with the excited state lifetime Γ^{-1}. If more levels are involved in the optical response, $h^{(2)}$ could become $h^{(2)} \gg 1$. Nevertheless in all cases there is a short time dynamics induced by the deviation from steady state, immediately following photon emission.

The above arguments apply for TLS with fixed parameters. Bath fluctuations on a timescale longer than Γ^{-1} cause another effect observed in SMS experiment. On this timescale the nonequilibrium effect of photon emission may be neglected, and the relaxation to a local steady state (with fixed system parameters) may be considered instantaneous.[38] The fluorescence trace is then a simple classical function of the bath state and may be used to directly probe bath dynamics. Periods of high and low fluorescence intensity are observed, often changing abruptly (blinking) which results in $h^{(2)} \gg 1$ (and superPoissonian photon distributions, bunching).

In Sec. 3 we show how multipoint correlation functions may be used to trace the microscopic origin of the relaxation processes.

Bulk spectroscopy is commonly performed in the weak field $\mu E \ll \Gamma$ (where μ is the dipole moment) regime to avoid saturation effects. In contrast, weak fields are not generally applicable to SMS experiments. Many photons should be recorded from a single-molecule source for good statistics. Many experiments are carried out using strong fields which may not be treated perturbatively. On the other hand, the weak field statistics, if accessible experimentally, may be easier to interpret. All moments simply scale with laser field intensity, e.g., $M \sim E^2$, and the linear regime may be simply controlled. The response can be described in terms of system characteristics and the magnitude of laser field enters as a simple prefactor.

A perturbative treatment of photon counting in the laser intensity should provide good insight into processes which may be probed by photon counting statistics. Consider a two-level system driven by a weak cw laser field

$$H_S = |e\rangle\omega_{eg}\langle e| - Ee^{-i\omega\tau}|e\rangle\mu\langle g| - E^*e^{i\omega\tau}|g\rangle\mu^*\langle e|.$$

The laser detuning from the two-level frequency ω_{eg} will be denoted by $\Delta \equiv \omega - \omega_{eg}$. The system interaction with bath degrees of freedom ($\mathbf{q}$) is described by the Hamiltonian

$$H_{SB} = |g\rangle H_g(\mathbf{q})\langle g| + |e\rangle H_e(\mathbf{q})\langle e|. \tag{13}$$

We further assume that the spontaneous emission rates are independent of the bath variables.

We define the dipole moment operator in the interaction picture

$$\begin{aligned} D_{eg}(\tau) &\equiv \mu \exp(iH_e\tau)\exp(-iH_g\tau); \\ D_{ge}(\tau) &\equiv \mu^* \exp(iH_g\tau)\exp(-iH_e\tau), \end{aligned} \tag{14}$$

and the corresponding superoperators $D_{eg}^{(L)}(\tau)\rho \equiv D_{eg}(\tau)\rho$; acting from the left (ket), and $D_{eg}^{(R)}(\tau)\rho \equiv \rho D_{eg}(\tau)$ acting from the right

(bra). The conjugate superoperators $D_{ge}(\tau)$ are defined in a similar manner.

The factorial moments and correlation functions may be described by double-sided Feynman diagrams which depict the evolution of the density matrix and are commonly used in nonlinear spectroscopy (see Figs. 1 and 2 for the lowest two factorial moments). Vertical lines represent the ket (left) or bra (right) of the density matrix, and assume the value e (excited state) or g (ground state). The following factors are assigned to the evolution during the time interval t: 1 for gg, $e^{-(i\Delta+\Gamma/2)t}$ for ge,$e^{(i\Delta-\Gamma/2)t}$ for eg, and $\exp(-\Gamma t)$ for ee. Additional factors are connected with the various interactions. The leading terms in the perturbative expansion for the kth correlation function $g^{(k)}$ are formed by the 2^k diagrams with k-bold horizontal

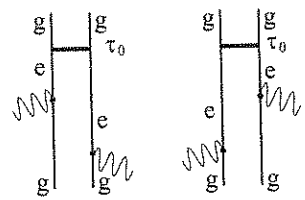

Fig. 1. Double-sided Feynman diagrams for steady-state fluorescence intensity to second (leading) order in the electric field (Eq. (15)).

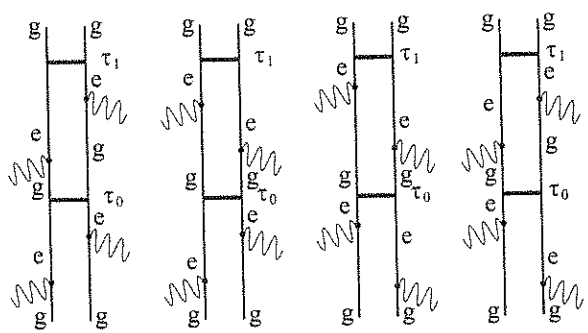

Fig. 2. Double-sided Feynman diagrams for the second factorial moment or two-point correlation function at steady state to fourth (leading) order in the electric field (Eq. (18)).

lines representing open photon detector and two (left and right) wavy lines between each pair of consecutive emissions representing interactions with the optical field, which induce the $g \to e$ transition. The interaction factors are $-iED_{eg}^{(L)}(\tau)$ for exciting ket, and $iE^*D_{ge}^{(R)}(\tau)$ for exciting bra. Bold horizontal line represents photon detection; change $ee \to gg$ and carries a factor $(\Gamma/|\mu|^2)D_{ge}^{(L)}(\tau)D_{eg}^{(R)}(\tau)$. (Due to the final tracing, the factors for the last emission are canceled since $\mathrm{Tr}\ D_{ge}^{(L)}(\tau)D_{eg}^{(R)}(\tau)\rho = |\mu|^2\ \mathrm{Tr}\ \rho$.) Rules for constructing the complete perturbative expansion may be found in Ref. 39. Strong field $\mu E \gg \Gamma$ counting statistics, nevertheless, should be rather calculated nonperturbatively starting from Eq. (9) (see discussion below).

For the correlation function $g^{(k)}$, the emission events are fixed at times $\tau_0, \ldots, \tau_k$, and the interactions are integrated over all times consistent with time ordering, as suggested by the respective diagrams. To calculate the factorial moments, the emission times need to be integrated as well over the binning times. The first two integrations must run from $-\infty$ (adiabatic switching) to build the steady state at τ_0.

We shall focus on the lowest two moments of photon counting. The fluorescence intensity and the average photon counting rate calculated to second order in the laser field assume the form (Fig. 1)

$$I=\Gamma E^2\int_{-\infty}^{0}d\tau_2'\int_{-\infty}^{\tau_2'}d\tau_1' e^{\Gamma\tau_2'}e^{(i\Delta-\Gamma/2)t_2'}\left\langle\!\left\langle D_{ge}^{(R)}(\tau_2')D_{eg}^{(L)}(\tau_1')\right\rangle\!\right\rangle_g + c.c., \tag{15}$$

and

$$\langle N\rangle(t) = \Gamma E^2\int_0^t d\tau_3'\int_{-\infty}^{\tau_3'}d\tau_2'\int_{-\infty}^{\tau_2'}d\tau_1' e^{-\Gamma t_3'}e^{(i\Delta-\Gamma/2)t_2'} \times\left\langle\!\left\langle D_{ge}^{(R)}(\tau_2')D_{eg}^{(L)}(\tau_1')\right\rangle\!\right\rangle_g + c.c., \tag{16}$$

with $t_j' \equiv \tau_j' - \tau_{j-1}'$. Brackets $\langle\langle\cdots\rangle\rangle \equiv \mathrm{Tr}\cdots\rho$ denote averaging where (superoperator) actions are in Liouville space. Equations (15) and (16) were obtained by direct application of the above rules. One integration in Eq. (15) and two of the integrations in Eq. (16) can be carried out to yield the classical formula for photon absorption[14]

$$\langle N\rangle(t) = It$$

with

$$I = E^2\int_0^\infty d\tau' e^{(i\Delta-\Gamma/2)\tau'}\langle\langle D_{ge}^{(R)}(\tau')D_{eg}^{(L)}(0)\rangle\rangle_g + c.c. \tag{17}$$

The linear absorption lineshape is thus determined by the autocorrelation function of the dipole operator, which depends on the dephasing on between two interactions with the laser field. The two-point correlation function is (Fig. 2)

$$\begin{aligned} g^{(2)}(t_1) = \frac{\Gamma^2E^4}{|\mu|^2}\int_0^{t_1}d\tau_5'\int_0^{\tau_5'}d\tau_4'\int_{-\infty}^{0}d\tau_2'\int_{-\infty}^{\tau_2'}d\tau_1' e^{-\Gamma(t_1-\tau_5'-\tau_2')} \\ \times\Big[e^{(i\Delta-\Gamma/2)t_5'}e^{(i\Delta-\Gamma/2)t_2'}\langle\langle D_{ge}^{(R)}(\tau_5')D_{eg}^{(L)}(\tau_4')D_{ge}^{(L)}(0) \\ \times D_{eg}^{(R)}(0)D_{ge}^{(R)}(\tau_2')D_{eg}^{(L)}(\tau_1')\rangle\rangle_g \\ + e^{(-i\Delta-\Gamma/2)t_5'}e^{(i\Delta-\Gamma/2)t_2'}\langle\langle D_{eg}^{(L)}(\tau_5')D_{ge}^{(R)}(\tau_4')D_{ge}^{(L)}(0) \\ \times D_{eg}^{(R)}(0)D_{ge}^{(R)}(\tau_2')D_{eg}^{(L)}(\tau_1')\rangle\rangle_g\Big] + c.c. \end{aligned} \tag{18}$$

The second factorial moment is

$$\begin{aligned} F^{(2)}(t) = 2\frac{\Gamma^2E^4}{|\mu|^2}\int_0^t d\tau_6'\int_0^{\tau_6'}d\tau_5'\int_0^{\tau_5'}d\tau_4' \\ \times\int_0^{\tau_4'}d\tau_3\int_{-\infty}^{\tau_3'}d\tau_2'\int_{-\infty}^{\tau_2'}d\tau_1' e^{-\Gamma(t_6'+t_3')} \\ \times\Big[e^{(i\Delta-\Gamma/2)t_5'}e^{(i\Delta-\Gamma/2)t_2'}\langle\langle D_{ge}^{(R)}(\tau_5')D_{eg}^{(L)}(\tau_4')D_{ge}^{(L)}(\tau_3') \\ \times D_{eg}^{(R)}(\tau_3')D_{ge}^{(R)}(\tau_2')D_{eg}^{(L)}(\tau_1')\rangle\rangle_g \\ + e^{(-i\Delta-\Gamma/2)t_5'}e^{(i\Delta-\Gamma/2)t_2'}\langle\langle D_{eg}^{(L)}(\tau_5')D_{ge}^{(R)}(\tau_4')D_{ge}^{(L)}(\tau_3') \\ \times D_{eg}^{(R)}(\tau_3')D_{ge}^{(R)}(\tau_2')D_{eg}^{(L)}(\tau_1')\rangle\rangle_g\Big] + c.c. \end{aligned} \tag{19}$$

Higher order correlation functions may be constructed in a similar manner. The Liouville-space correlation functions Eqs. (16)–(18) may be recast in terms of ordinary (Hilbert space) dipole correlation functions (brackets $\langle \cdots \rangle$ denote averaging where the operators act in Hilbert space). We get

$$\left\langle\left\langle D_{ge}^{(R)}(\tau_2) D_{eg}^{(L)}(\tau_1)\right\rangle\right\rangle_g = J(\tau_2, \tau_1),$$

where

$$J(\tau_2, \tau_1) \equiv \langle D_{ge}(\tau_2) D_{eg}(\tau_1)\rangle_g.$$

Similarly, we introduce the six-point correlation function

$$\begin{aligned} &F(\tau_1, \tau_2, \tau_3, \tau_4, \tau_5, \tau_6) \\ &\quad \equiv \langle D_{ge}(\tau_1) D_{eg}(\tau_2) D_{ge}(\tau_3) D_{eg}(\tau_4) D_{ge}(\tau_5) D_{eg}(\tau_6)\rangle_g. \end{aligned}$$

We then have

$$\begin{aligned} &\left\langle\left\langle D_{ge}^{(R)}(\tau_5) D_{eg}^{(L)}(\tau_4) D_{ge}^{(L)}(\tau_3) D_{eg}^{(R)}(\tau_3) D_{ge}^{(R)}(\tau_2) D_{eg}^{(L)}(\tau_1)\right\rangle\right\rangle_g \\ &\quad = F(\tau_2, \tau_3, \tau_5, \tau_4, \tau_3, \tau_1), \\ &\left\langle\left\langle D_{eg}^{(L)}(\tau_5) D_{ge}^{(R)}(\tau_4) D_{ge}^{(L)}(\tau_3) D_{eg}^{(R)}(\tau_3) D_{ge}^{(R)}(\tau_2) D_{eg}^{(L)}(\tau_1)\right\rangle\right\rangle_g \\ &\quad = F(\tau_2, \tau_3, \tau_4, \tau_5, \tau_3, \tau_1). \end{aligned}$$

In Liouville space we only require forward time ordering. The related Hilbert space correlation functions have a more complex structure for time orderings, because they mix the forward time orderings for the ket and backward orderings for the bra. For the spin boson model[14] these correlation functions may be exactly calculated in a closed form using the second-order cumulant expansion.[39]

We now explain the physical significance of Eq. (18). The molecule, initially ($\tau = -\infty$) at equilibrium in the ground state, interacts with the electric field, via the bra (from the right) $D_{ge}^{(R)}$, and the ket (left) $D_{eg}^{(L)}$ at times τ_1' and τ_2', respectively. The propagation in $|ge\rangle\rangle$ or $|eg\rangle\rangle$ between τ_1' and τ_2' (i.e. the interval t_2') includes the decay $e^{-\Gamma t_2'/2}$, and the propagation in $|ee\rangle\rangle$ between τ_2' and $\tau_0 = 0$ includes $e^{-\Gamma \tau_2'}$ representing the excited state lifetime. The density matrix at

$\tau_0 = 0$ represents the steady state, and the average photon count (Eq. (16)) is obtained at this point. At $\tau_0 = 0$ we observe the emitted photon and the molecule moves to the ground state described by the factors $D_{ge}^{(L)}(\tau_0) D_{eg}^{(R)}(\tau_0)$. The excitation at times τ_4' and τ_5', and the second emission at time τ_1 can be described in a similar way. Following the emission at τ_0, the molecule is no longer at equilibrium in the ground state. Its state depends on the spontaneous emission rate, the relaxation rate, and laser detuning. Thus, correlations build up and the probability of subsequent absorption from the initial state may be different.

The fully microscopic expressions given above include a proper description of bath reorganization and the effects of resetting. The connection between nonlinear spectroscopy and SMS for classical stochastic ω_{eg} fluctuations applied to the weak field counting formula Eq. (32) was discussed in Refs. 40 and 41. This approach neglects antibunching (valid for the long time limit) induced by the resetting, some unphysical Hilbert space time orderings of D_{eg} operators contribute, which never show up in the full microscopic derivation, and the Stokes shift is neglected. The stochastic Liouville equations provide a different approach to SMS photon counting statistics.[36] They rigorously incorporate Markovian stochastic ω_{eg} fluctuations into the full Liouville Equations Eq. (8) and resolve the first two difficulties. It has two important additional advantages: it allows a nonperturbative treatment in the electric field because it may be often expanded in finite dimensional linear space and is therefore applicable to strong fields. Photon counting observables for non-Gaussian fluctuations may then be calculated exactly. On the other hand, the SLE misses finite temperature effects. Bath reorganization and the Stokes shift are neglected since the bath evolution is independent of the state of the system.[42] For the spin-boson model of bath fluctuations, Eq. (13) may be expanded as a sum of stochastic coordinates, and should include some temperature correction terms [42, 61]. The stochastic Liouville equations are recovered in the high temperature limit. The first correction introduce a Stokes shift between the ground state and excited state harmonic surface. Further corrections

may systematically bring in additional oscillators, whose Matsubara frequencies depend on temperature. This connects the SLE with the microscopic spin-boson bath model, and suggests a practical nonperturbative way for calculating strong field effects.

To compare the microscopic expressions with the SLE approach we note that for classical stochastic models, the left (ket) and the right (bra) bath density matrix variables are identical, and may be considered as stochastic c-number variables ($D_{ge}(\tau) = D^*_{eg}(\tau)$) rather than operators in the bath Hilbert space. The factor corresponding to emission is thus eliminated,

$$(1/|\mu|^2)D^{(L)}_{ge}(\tau)D^{(R)}_{eg}(\tau) \to (1/|\mu|^2)D^*_{eg}(\tau)D_{eg}(\tau) = 1, \qquad (20)$$

and the six-point correlation function reduces to a four-point function. The two-point correlation function becomes

$$\begin{aligned} g^{(2)}(t_1) = \frac{\Gamma^2 E^4}{|\mu|^2}\int_0^{t_1} d\tau_5' \int_0^{\tau_5'} d\tau_4' \int_{-\infty}^{0} d\tau_2' \int_{-\infty}^{\tau_2'} d\tau_1' e^{-\Gamma(t_1-\tau_5'-\tau_2')} \\ \times \Big[e^{(i\Delta-\Gamma/2)t_5'} e^{(i\Delta-\Gamma/2)t_2'} \langle\langle D_{ge}(\tau_5') D_{eg}(\tau_4') \\ \times D_{ge}(\tau_2') D_{eg}(\tau_1')\rangle\rangle_g + e^{(-i\Delta-\Gamma/2)t_5'} e^{(i\Delta-\Gamma/2)t_2'} \\ \times \langle\langle D_{eg}(\tau_5') D_{ge}(\tau_4') D_{ge}(\tau_2') D_{eg}(\tau_1')\rangle\rangle_g \Big] + c.c. \end{aligned} \qquad (21)$$

The time variable associated with the emission event in Eq. (19) can be integrated out, giving

$$\begin{aligned} F^{(2)}(t) = 2E^4(\Gamma/|\mu|)^2 \int_0^{t} d\tau_4' \int_0^{\tau_4'} d\tau_3 \int_{-\infty}^{\tau_3'} d\tau_2' \int_{-\infty}^{\tau_2'} d\tau_1 \\ \times (\xi(\tau_2') - e^{-\Gamma t_3'})(1 - e^{-\Gamma(t-\tau_4')}) e^{(i\Delta-\Gamma/2)t_2'} \\ \times \Big[e^{(i\Delta-\Gamma/2)t_4'} \langle D_{ge}(\tau_4') D_{eg}(\tau_3') D_{ge}(\tau_2') D_{eg}(\tau_1')\rangle \\ + e^{(-i\Delta-\Gamma/2)t_4'} \langle D_{ge}(\tau_4') D_{eg}(\tau_2') D_{ge}(\tau_4') D_{eg}(\tau_3')\rangle \Big] + c.c., \end{aligned} \qquad (22)$$

where $\xi(t) = 1$ for $t > 0$ and $\exp(\Gamma t)$ for $t < 0$.

We next compare these results with the coherent four-wave mixing response which depends on similar correlation functions. In ultrafast nonlinear spectroscopy three laser pulses (with wavevectors $\mathbf{k_1}, \mathbf{k_2}, \mathbf{k_3}$) interact with the probed molecule at prescribed times. Spatial coherence is retained, and the response to laser pulses is observed in specific phase-matching directions. Combining signals from various directions allows to select a specific Liouville space pathway which represents the evolution of the molecule density nature during the course of the experiment. The signal generated in the $\mathbf{k_I} = \mathbf{k_1} + \mathbf{k_2} + \mathbf{k_3}$ (photon echo) phase matching direction is[14]

$$\begin{aligned} S_{\rm I}(t_3, t_2, t_1) = \left(\frac{i}{\hbar}\right)^3 e^{-i\omega_{eg}t_3} e^{i\omega_{eg}t_1} \\ \times \left(\left\langle\!\left\langle D^{(L)}_{ge}(\tau_3) D^{(L)}_{eg}(\tau_2) D^{(R)}_{eg}(\tau_1) D^{(R)}_{ge}(\tau_0)\right\rangle\!\right\rangle_g \right. \\ \left. + \left\langle\!\left\langle D^{(L)}_{ge}(\tau_3) D^{(R)}_{eg}(\tau_2) D^{(L)}_{eg}(\tau_1) D^{(R)}_{ge}(\tau_0)\right\rangle\!\right\rangle_g \right) + c.c., \end{aligned} \qquad (23)$$

and for the $\mathbf{k_{II}} = \mathbf{k_1} - \mathbf{k_2} + \mathbf{k_3}$ direction we get

$$\begin{aligned} S_{\rm II}(t_3, t_2, t_1) = \left(\frac{i}{\hbar}\right)^3 e^{-i\omega_{eg}t_3} e^{-i\omega_{eg}t_1} \\ \times \left(\left\langle\!\left\langle D^{(L)}_{ge}(\tau_3) D^{(L)}_{ge}(\tau_2) D^{(L)}_{ge}(\tau_1) D^{(L)}_{eg}(\tau_0)\right\rangle\!\right\rangle_g \right. \\ \left. + \left\langle\!\left\langle D^{(L)}_{ge}(\tau_3) D^{(R)}_{eg}(\tau_2) D^{(R)}_{ge}(\tau_1) D^{(L)}_{eg}(\tau_0)\right\rangle\!\right\rangle_g \right) + c.c. \end{aligned} \qquad (24)$$

Photon counting and nonlinear spectroscopy are thus related to the same type of correlation functions, but on very different timescales: miliseconds vs femtoseconds, respectively. We assume $\Gamma = 0$ in Eqs. (23) and (24) because spontaneous emission is less important at femtosecond timescale.

Finally we note that similar correlation functions also appear in the description of time- and frequency-resolved fluorescence[43]

$$\begin{aligned} S(\omega_L, \omega_S, t) = \frac{2}{\hbar^2}{\rm Re}[S_1(\omega_L, \omega_S, t) + S_2(\omega_L, \omega_S, t) \\ + S_3(\omega_L, \omega_S, t)], \end{aligned} \qquad (25)$$

where ω_L is the laser frequency, ω_S the fluorescence frequency, and

$$S_1(\omega_L,\omega_S,t)=\int_0^\infty d\tau\int_{-\infty}^{t-\tau}d\tau_1\int_{-\infty}^{\tau_1}d\tau_2 e^{-i\omega_S\tau}e^{-i\omega_L(\tau_1-\tau_2)}\times e^{-\Gamma(\tau+\tau_1-\tau_2)/2}\left\langle\!\left\langle D_{ge}^{(L)}(t)D_{eg}^{(R)}(t-\tau)D_{ge}^{(R)}(\tau_1)\times D_{eg}^{(L)}(\tau_2)\right\rangle\!\right\rangle_g E(\tau_1)E^*(\tau_2) \quad (26)$$

$$S_2(\omega_L,\omega_S,t)=\int_0^\infty d\tau\int_{-\infty}^{t-\tau}d\tau_2\int_{-\infty}^{\tau_2}d\tau_1 e^{-i\omega_S\tau}e^{-i\omega_L(\tau_1-\tau_2)}\times e^{-\Gamma(\tau+\tau_2-\tau_1)/2}\left\langle\!\left\langle D_{ge}^{(L)}(t)D_{eg}^{(R)}(t-\tau)D_{eg}^{(L)}(\tau_2)\times D_{ge}^{(R)}(\tau_1)\right\rangle\!\right\rangle_g E(\tau_1)E^*(\tau_2) \quad (27)$$

$$S_3(\omega_L,\omega_S,t)=\int_{-\infty}^{t}d\tau_2\int_{t-\tau_2}^\infty d\tau\int_{-\infty}^{t-\tau}d\tau_1 e^{-i\omega_S\tau}e^{-i\omega_L(\tau_1-\tau_2)}\times e^{-\Gamma(2t-\tau-\tau_1-\tau_2)/2}\left\langle\!\left\langle D_{ge}^{(L)}(t)D_{eg}^{(L)}(\tau_2)D_{eg}^{(R)}(t-\tau)\times D_{ge}^{(R)}(\tau_1)\right\rangle\!\right\rangle_g E(\tau_1)E^*(\tau_2). \quad (28)$$

Unlike coherent nonlinear signals, fluorescence emissions are nondirectional (i.e. not phase-matched).

3. Multipoint correlation functions for slow fluctuations

Slow environment fluctuations in many SMS experiments may be analyzed using multipoint correlation functions of some classical stochastic coordinate x.[6,11–13] Various microscopic models which share the same two-point correlation functions may be distinguished through their higher order correlation functions. We consider an SMS observable given by a multipoint correlation function of a function $f(x)$ of such coordinate x

$$g_f^{(k+1)}(t_k,\ldots,t_1)=\langle f(x(\tau_k))\cdots f(x(\tau_0))\rangle, \quad (29)$$

where $t_j\equiv\tau_j-\tau_{j-1}$ are the time intervals. By expanding $f(x)$ in a Taylor series $f(x)=\sum_l f_l x^l$, we can recast it in terms of multipoint correlation functions of x

$$g_f^{(k+1)}(t_k,\ldots,t_1)=\sum_{l_0}\cdots\sum_{l_k}f_{l_0}\cdots f_{l_k}\langle x^{l_k}(\tau_k)\cdots x^{l_0}(\tau_0)\rangle.$$

The most detailed description of a k-point measurement is given by the probability density function (PDF)

$$P^{(k+1)}(\tau_k y_k,\ldots,\tau_0 y_0)\equiv\langle\delta(y_k-x(\tau_k))\cdots\delta(y_0-x(\tau_0))\rangle. \quad (30)$$

Multipoint correlation functions are given by moments of the PDFs

$$g_f^{(k+1)}(t_k,\ldots,t_1)=\sum_{y_k}\cdots\sum_{y_0}f(y_k)\cdots f(y_0)\times P^{(k+1)}(\tau_k y_k,\ldots,\tau_0 y_0). \quad (31)$$

When the moment-generating function

$$\zeta(\xi_k,\ldots,\xi_0)\equiv\sum_{l_0=0}^\infty\cdots\sum_{l_k=0}^\infty\frac{(\xi_k)^{l_k}}{l_k!}\cdots\frac{(\xi_0)^{l_0}}{l_0!}\langle x^{l_k}(\tau_k)\cdots x^{l_0}(\tau_0)\rangle=\left\langle\exp\left(\sum_j\xi_j x(\tau_j)\right)\right\rangle$$

converges around $\zeta=0$, the PDFs can be obtained by inverse Laplace transform

$$P^{(k+1)}(\tau_k y_k,\ldots,\tau_0 y_0)=\int_{-i\infty}^{i\infty}d\xi_0\cdots\int_{-i\infty}^{i\infty}d\xi_k e^{-(\xi_0 y_0+\cdots+\xi_k y_k)}\zeta(\xi_k,\ldots,\xi_0).$$

For a certain class of dynamic models, the PDFs can thus be obtained from the complete set of correlation functions. However, the moments

do not always exist and the moment-generating function may not converge. In this sense PDFs are more general than moments. Lower moments are more accessible experimentally, because measuring higher moments or the PDF itself requires more extensive sampling.

We shall examine two examples of SMS observables described by correlation functions of a classical coordinate.

1. Multipoint correlation functions $g_I^{(k)}$ of fluorescence intensities. We consider a resonantly pumped two-level chromophore, whose transition frequency undergoes slow stochastic fluctuations $\delta\omega$. The time-dependent fluorescence intensity is

$$I(\delta\omega) = \frac{(\mu E)^2}{(\mu E)^2 + \Gamma^2 + \delta\omega^2},$$

where μE is the Rabi frequency. We assume that the fluorescence quantum yield does not fluctuate so that the fluorescence intensity is proportional to the absorption. $\delta\omega$ is a classical coordinate, whose dynamics and correlations may be probed through multipoint correlations of time- and frequency-resolved fluorescence intensities

$$g_I^{(k+1)}(t_k, \ldots, t_1) = \langle I(\delta\omega(\tau_k)) \cdots I(\delta\omega(\tau_0))\rangle. \qquad (32)$$

2. Photon arrival trajectories (PAT).[44,45] The molecule is excited by a train of laser pulses and after each pulse one or no photon is emitted. The delays of emitted photons with respect to each pulse are recorded (Fig. 3). These delays depend on the competition between photon emission and quenching. We consider a chromophore and a quencher attached to a polymer (e.g., an enzyme).

Fig. 3. Photon arrival experiment. Train of pulses at times τ_j excites the molecule. The time delays T_j between the photon arrival time and the exciting pulse at τ_j are recorded. Some excitations are not followed by a response, such as the pulse τ_4. According to our definition this path does not contribute to $P^{(2)}(\tau_4, \tau_1)$ etc.

Conformational dynamics thus affects the quenching rate. Increasing the quenching rate affects the photon arrival statistics in two ways: faster arrival times and lower fluorescence yield. The $(k+1)$-time photon arrival joint function $P^{(k+1)}(T_k\tau_k, \ldots, T_0, \tau_0)_T$ considered here may be calculated solely from the experimentally accessible photon trajectories where a photon is observed after each of the incoming pulses at $\tau_0, \ldots, \tau_k$ (T ensemble). The trajectories where photon was not recorded after some of the pump pulses $\tau_0, \ldots, \tau_k$ are not included. The observable is the correlation function

$$g_T^{(k+1)}(t_k, \ldots, t_1) \equiv \langle T(\tau_k) \cdots T(\tau_0)\rangle_T, \qquad (33)$$

where the photon arrival time $T(\tau_k)$ is the delay between the kth excitation pulse and the detected photon, and $t_j \equiv \tau_j - \tau_{j-1}$ are intervals between pulses. Excitation quenching shortens its lifetime and the average photon arrival time. When the quenching rate is determined by a donor–acceptor distance Q, the photon arrival time may be mapped into the statistics of Q. The two common quenching mechanisms are fluorescence resonance energy transfer (FRET) $\gamma_{\text{FRET}} = k_{\text{FRET}}(R_0/Q)^6$, where R_0 is the Förster radius,[46] and electron transfer (ET) $\gamma_{\text{ET}} = k_{\text{ET}} \exp(-\beta Q)$.[44] The total fluorescence decay rate is $\gamma(t) = [\gamma_0 + \gamma_j(Q(t))]$, where γ_0 is the radiative rate and γ_j (j = FRET or ET) is the quenching rate.

We next turn to the photon arrival time statistics. The probability density function for the photon arrival trajectory is generally given by a path integral

$$P^{(k+1)}(\tau_k T_k, \ldots, \tau_0 T_0)_T$$

$$= C_{k+1}^{-1} \langle e^{-\int_0^{T_k} \gamma(Q(\tau_k + t'))dt'} \cdots e^{-\int_0^{T_0} \gamma(Q(\tau_0 + t'))dt'} \rangle_Q, \qquad (34)$$

where

$$C_{k+1} = \int \cdots \int \langle e^{-\int_0^{T_k} \gamma(Q(\tau_k + t'))dt'} \cdots e^{-\int_0^{T_0} \gamma(Q(\tau_0 + t'))dt'} \rangle_Q \times dT_k \cdots dT_0$$

is the normalization factor. $\langle\,\rangle_Q$ denotes ensemble averaging over all trajectories of the stochastic coordinate. It differs from the T ensemble since the quantum yield decreases with quenching rate, and trajectories with high quenching are underrepresented in the T ensemble.

Evaluating the right-hand side of Eq. (34) requires a path integral over trajectories $Q(t)$. In Sec. 3.2, we shall evaluate it for small Gaussian fluctuations where γ depends linearly on Q. This model is exactly solvable using the second-order cumulant expansion. The calculation is considerably simplified for slow fluctuations whereby Q does not change during the decay time of single excitation and we can set $Q(\tau_k + t') \approx Q(\tau_k)$. The path integral equation (34) then reduces to a k-point correlation function

$$P^{(k+1)}(\tau_k T_k, \ldots, \tau_0 T_0)_T = C_{k+1}^{-1} \left\langle e^{-\gamma(Q(\tau_k))T_k} \cdots e^{-\gamma(Q(\tau_0))T_0} \right\rangle_Q \tag{35}$$

and

$$C_{k+1} = \langle \gamma^{-1}(Q(\tau_k)) \cdots \gamma^{-1}(Q(\tau_0)) \rangle_Q.$$

Since the summations (integrations) over T in Eq. (31) lead to various inverse powers of γ, we define $\varphi \equiv \gamma^{-1}$. The correlation function (Eq. (33)) is given by

$$g_T^{(k+1)}(t_k, \ldots, t_1) = \frac{\langle \varphi^2(Q(\tau_k)) \cdots \varphi^2(Q(\tau_0)) \rangle_Q}{\langle \varphi(Q(\tau_k)) \cdots \varphi(Q(\tau_0))) \rangle_Q}.$$

In the slow fluctuation limit we can thus recast the averaging over photon arrivals in terms of quenching rate fluctuations. When these fluctuations are small compared to the mean quenching rate, the variation of the quantum yield with quenching rate is commonly ignored and the correlation of arrival times $\delta T \equiv T - \bar{T}$; $\bar{T} \equiv \langle T \rangle_T$ is by the inverse decay rates $\delta\varphi \equiv \varphi - \langle \varphi \rangle_Q$:

$$g_{\delta T}^{(k+1)}(t_k, \ldots, t_1) = \langle \delta T(\tau_k) \cdots \delta T(\tau_0) \rangle_T \sim \langle \delta\varphi(\tau_k) \cdots \delta\varphi(\tau_0) \rangle_Q$$

$$= g_{\delta\varphi}^{(k+1)}(t_k, \ldots, t_1). \tag{36}$$

In this approximation correlations of photon arrival times coincide with those of the lifetime. Equation (36) has been used in the modeling of single-molecule FRET and ET experiments.[6,11,47]

A formal relation may be derived by perturbative expansion in $\delta\varphi$ of $\bar{T} = \langle \varphi^2(Q) \rangle_Q / \langle \varphi(Q) \rangle_Q$ and

$$\begin{aligned} \langle \delta T(\tau_1) \delta T(\tau_0) \rangle_T = C_2^{-1} \big(& \langle \varphi^2(Q(\tau_1)) \varphi^2(Q(\tau_0)) \rangle_Q \\ & - \bar{T} \langle \varphi^2(Q(\tau_1)) \varphi(Q(\tau_0)) \rangle_Q \\ & - \bar{T} \langle \varphi(Q(\tau_1)) \varphi^2(Q(\tau_0)) \rangle_Q \big) + \bar{T}^2. \end{aligned} \tag{37}$$

Note that the average $C_2^{-1} \langle \varphi^2(Q(\tau_1)) \varphi(Q(\tau_0)) \rangle_Q \neq T$ may not be simply reduced to $\bar{T}$ even though it represents an average arrival time at τ_1, since the averaging is performed over paths where a photon is detected both at τ_0 and τ_1. This is different from the averaging over paths with a photon detected at τ_1, which is required for $\bar{T}$. Even though the leading terms in the expansion $\delta\varphi$ for two-point correlations recover Eq. (36), for higher order quantities it can be violated as we show for Gaussian modulation of ET quenching case in Sec. 3.2. Therefore, Eq. (36) needs to be used with some caution.

Note that PDFs of Q are less accessible experimentally than correlation functions. Because of the stochastic nature of photon emission a large number of photon arrival events must be recorded before Q is changed, for a proper sampling of the quenching rate at given Q. This is a much stronger condition than the stationarity of Q during a single emission event, assumed in Eq. (35).

When γ_0 is small, the correlation functions (Eq. (33)) reduce to simple functional forms such as $\langle e^{-\beta Q(\tau_k)} \cdots e^{-\beta Q(\tau_0)} \rangle$ (ET) and $\langle Q^6(\tau_k) \cdots Q^6(\tau_0) \rangle$ (FRET). In either case we can relate the multipoint correlation functions of the photon arrival trajectory to correlation functions of a stochastic coordinate Q. In some special cases the two-point Green function completely characterizes the process. The higher, multipoint, quantities provide additional information that may be used to test the validity of various models. Below we discuss how these multipoint correlation functions

may be used to characterize the nature of bath relaxation. Three approaches for modeling the dynamics will be surveyed.

3.1. *Markovian dynamics*

A Markovian description is possible when the state of the system is fully characterized by a few collective variables, and the future evolution of the system only depends on their current values. The probability for a path $x(\tau)$ for $\tau > 0$ starting at $x(0)$ is independent of its past history $\tau < 0$. The dynamics is then described by simple rate equations and all necessary information is contained in the two-point Green function $G(\tau_j x_j, \tau_{j-1} x_{j-1})$. The joint PDF may be calculated as à product of two-point Green functions

$$P^{(k+1)}(\tau_k x_k, \ldots, \tau_0 x_0) = G(\tau_k x_k, \tau_{k-1} x_{k-1}) \cdots G(\tau_1 x_1, \tau_0 x_0) \rho(x_0, \tau_0). \quad (38)$$

Two-point Green functions of a Markovian process must satisfy the Chapman–Kolmogorov equation

$$G(\tau_2 x_2, \tau_0 x_0) = \int dx_1 G(\tau_2 x_2, \tau_1 x_1) G(\tau_1 x_1, \tau_0 x_0). \quad (39)$$

For discrete variables, G may be viewed as a matrix with indices x_n and x_{n-1}, and Eq. (39) should be interpreted as a matrix product. The Markovian property is built-in: the probabilities of the $x_0 \to x_1$ and the $x_1 \to x_2$ moves are independent; the probability of the entire trajectory is simply the product of probabilities of its two segments. The integration over x_1 in Eq. (39) indicates going from x_0 to x_2 through all possible values x_1. If the process is stationary, Green's function depends only on the time intervals $t_j = \tau_j - \tau_{j-1}$ and defines a one-parameter semigroup. It can be expressed via operator exponential correlation functions of a Markovian process, characterized by multi-exponential decays.

It should be noted that Markovian dynamics is not merely an intrinsic property of a given physical process, but rather depends on the chosen level of description. Some processes may become Markovian when the system's description is expanded by including additional degrees of freedom, which otherwise cause memory effects. When reducing the amount of information kept on the system, i.e. projecting-off some bath degrees of freedom, the description becomes nonMarkovian and memory effects build up. Formal extension to a Markovian description is often a reasonable strategy for theoretical modeling. The evolution of a fluctuating quantum system is then fully described by the two-point Green function. Similar strategy was used in Sec. 1 of this chapter. In practice it makes sense to denote the process "Markovian" only when a Markovian description is possible using a few, preferably experimentally accessible, degrees of freedom.

One common Markovian model which involves discrete multistate jumps (known from lineshapes theory) has been utilized to describe blinking between several fluorescence intensity levels.

Consider the simplest model of two states d and u, given its master equation

$$\frac{d\rho}{dt} = \hat{W}\rho; \quad \hat{W} = \begin{pmatrix} -\Lambda_u & \Lambda_d \\ \Lambda_u & -\Lambda_d \end{pmatrix};$$

and its Green function solution

$$\hat{G}(t) = \exp[\hat{W}t] = \hat{1} + \frac{1 - \exp[-(\Lambda_u + \Lambda_d)t]}{\Lambda_u + \Lambda_d} \hat{W}. \quad (40)$$

We shall next denote φ in state u and d as φ_u and φ_d, respectively, e.g., for ET, $\varphi_u = \exp(\beta Q_u)$.

Below we present the first three PAT correlation functions in the slow limit

$$g_T^{(1)} = \langle T \rangle_T = \frac{\Lambda_u \varphi_u^2 + \Lambda_d \varphi_d^2}{\Lambda_u \varphi_u + \Lambda_d \varphi_d}$$

$$g_T^{(2)}(t_1) = \frac{\Lambda_d \varphi_d^4 + \Lambda_d \varphi_d^4 - s(t_1) \Lambda_u \Lambda_d (\varphi_u^2 - \varphi_d^2)^2}{\Lambda_d \varphi_d^2 + \Lambda_d \varphi_d^2 - s(t_1) \Lambda_u \Lambda_d (\varphi_u - \varphi_d)^2},$$

where we denoted $s(t) \equiv (1 - \exp[-(\Lambda_u + \Lambda_d)t])/(\Lambda_d + \Lambda_u)$, and

$$g_T^{(3)}(t_2, t_1) = \frac{\begin{array}{c}\Lambda_d\varphi_d^6 + \Lambda_u\varphi_u^6 + \Lambda_u\Lambda_d[(s(t_1) + s(t_2))(\varphi_d^4\varphi_u^2 + \varphi_u^4\varphi_d^2 - \varphi_u^6 \\ - \varphi_d^6) + s(t_1)s(t_2)(\varphi_u^2 - \varphi_d^2)^2(\Lambda_u\varphi_d^2 + \Lambda_d\varphi_u^2)]\end{array}}{\begin{array}{c}\Lambda_d\varphi_d^3 + \Lambda_u\varphi_u^3 + \Lambda_u\Lambda_d[(s(t_1) + s(t_2))(\varphi_d^2\varphi_u + \varphi_u^2\varphi_d \\ - \varphi_u^3 - \varphi_d^3) + s(t_1)s(t_2)(\varphi_u - \varphi_d)^2(\Lambda_u\varphi_d + \Lambda_d\varphi_u)]\end{array}}.$$

Beyond the slow limit the path integral equation (34) may be readily calculated using the stochastic Liouville equations.[42] To do this the time evolution need to be separated for the two types of intervals. Between $\tau_{j-1} + T_{j-1}$ and τ_j the generating function is given by Eq. (40). For the intervals between τ_j and T_j, generating function $\hat{G}^\gamma$ must account for the quenching

$$\hat{G}^\gamma(t) = \exp\left[\begin{pmatrix} -k_u - \gamma_d & k_d \\ k_u & -k_d - \gamma_u \end{pmatrix} t\right],$$

and the PDFs are given by their ordered product

$$P^{(k+1)}(T_k\tau_k, \ldots, T_1\tau_1, T_0\tau_0) = \mathrm{Tr}\,\hat{G}^\gamma(T_j)\hat{G}(t_k - T_{k-1})\cdots\hat{G}(t_1 - T_0)\hat{G}^\gamma(T_0)\rho(0).$$

PDFs and correlation functions may be readily calculated using elementary algebra, however, the final expressions are rather lengthy.

Another common model is a random walk in a potential described by the Fokker–Planck equation[48]

$$\frac{d\rho(r,t)}{dt} = \Lambda\left[\frac{\partial^2}{\partial x^2} - \frac{\partial}{\partial x}\frac{F(x)}{\mathbf{kT}}\right]\rho(r,t), \tag{41}$$

where Λ is the relaxation rate, $\mathbf{T}$ is the temperature, and F is the force. For a harmonic force $F(x) = -\mathcal{M}\Omega^2 x$, the Green function of the Fokker–Planck equation (41) is

$$G(\tau_{j+1}x_{j+1};\tau_j x_j) \equiv \sqrt{\frac{\mathcal{M}\Omega^2}{2\mathbf{kT}\pi(1 - e^{-2\Lambda(\tau_{j+1}-\tau_j)})}} \times \exp\left[\frac{-\mathcal{M}\Omega^2(x_{j+1} - e^{-\Lambda(\tau_{j+1}-\tau_j)}x_j)^2}{2\mathbf{kT}(1 - e^{-2\Lambda(\tau_{j+1}-\tau_j)})}\right] \tag{42}$$

and the equilibrium distribution

$$\rho(x_0) = \sqrt{\frac{\mathcal{M}\Omega^2}{2\mathbf{kT}\pi}}\exp\left[\frac{-\mathcal{M}\Omega^2}{2\mathbf{kT}}x_0^2\right]. \tag{43}$$

Equations (42) and (43) show that this is special case of Gaussian process, which will be described in the next section, where we also provide the correlation functions for PAT with ET quenching.

3.2. *Gaussian dynamics*

Consider a harmonic oscillator x coupled to a harmonic bath with coordinates q_j. The system is described by the Hamiltonian

$$H = \frac{p^2}{2\mathcal{M}} + \frac{\mathcal{M}\Omega^2 x^2}{2} + \sum_j\left[\frac{p_j^2}{2m_j} + \frac{m_j\omega_j^2}{2}\left(q_j - \frac{c_j}{m_j\omega_j^2}x\right)^2\right]. \tag{44}$$

x may be viewed as a collective coordinate given by a linear combination of the normal modes of H.[49] All correlation functions for this model may be obtained in a single step using the generating functional technique described below.

Quantum evolution may not be described by trajectories; each value ascribed to some observable should be established by a measurement, which necessarily changes the state of the system.[49] In general, quantum correlation functions of x are not directly relevant for the description of multipoint measurements since they do

not include the effect of wavefunction collapse accompanying a quantum measurement. The quantum-classical correspondence may be established by adopting a semiclassical description through the Wigner distribution function, and the measurement is represented by superoperator action in Liouville space $X_+\rho = (x\rho + \rho x)/2$, i.e. $X_+ = (X^{(L)} + X^{(R)})/2$. A classical measurement is thus related to $\delta(X_+ - x)$.

All quantities of interest may be derived from the generating functional

$$\mathcal{S}(J) \equiv \left\langle \mathcal{T} \exp\left[-i \int_0^t d\tau (J(\tau) X_+(\tau))\right]\right\rangle, \tag{45}$$

where $\mathcal{T}$ is a time ordering operation of superoperators. In the classical limit it reads

$$\mathcal{S}(J) \equiv \left\langle \exp\left[-i \int_0^t d\tau (J(\tau) x(\tau) d\tau)\right]\right\rangle. \tag{46}$$

The model defined by Eq. (44) is exactly solvable. The exact generating functional is obtained by the second-order cumulant expansion

$$\mathcal{S}(J) = \exp\left[\int_0^t d\tau'' \int_0^t d\tau' \left(-\frac{1}{2} g_x^{(2)}(\tau'' - \tau') J(\tau'') J(\tau')\right)\right], \tag{47}$$

where T is the temperature, and the correlation function

$$g_x^{(2)}(t) = \hbar \int_{-\infty}^{\infty} \frac{d\omega}{2\pi} \cos(\omega t) \coth\left(\frac{\hbar\omega}{2\mathbf{kT}}\right) C(\omega).$$

All relevant information is contained in the spectral density $C(\omega)$ of the collective coordinate which determines the two-point correlation functions $g_x^{(2)}$[14,50,51]:

$$C(\omega) = \frac{1}{\mathcal{M}} \frac{\omega \upsilon(\omega)}{(\Omega^2 + \omega\Sigma(\omega) - \omega^2)^2 + \omega^2 \upsilon^2(\omega)}, \tag{48}$$

where

$$\upsilon(\omega) = \frac{\pi}{\mathcal{M}} \sum_j \frac{c_j^2}{2m_j\omega_j^2} \left[\delta(\omega - \omega_j) + \delta(\omega + \omega_j)\right]. \tag{49}$$

Σ and υ are related by the Kramers–Kronig relation

$$\Sigma(\omega) = -\frac{1}{\pi} pp \int_{-\infty}^{\infty} d\omega' \frac{\upsilon(\omega')}{\omega' - \omega}. \tag{50}$$

The classical model is recovered in the high-temperature limit by retaining the first term in the expansion

$$\hbar \coth\left(\frac{\hbar\omega}{2\mathbf{kT}}\right) = \frac{2\mathbf{kT}}{\omega} + \frac{\hbar^2\omega}{6\mathbf{kT}} - \frac{\hbar^4\omega^3}{360(\mathbf{kT})^3} + \cdots \tag{51}$$

This gives

$$g_x^{(2)}(t) = \int_{-\infty}^{\infty} \frac{d\omega}{2\pi} \cos(\omega t) \left(\frac{2\mathbf{kT}}{\omega}\right) C(\omega). \tag{52}$$

Correlation functions are obtained by functional differentiation with respect to $J(t)$, and setting $J = 0$

$$\langle x(\tau_k) \cdots x(\tau_0)\rangle = i^k \frac{\delta \mathcal{S}(J)}{\delta J(\tau_k) \cdots \delta J(\tau_0)}\bigg|_{J=0}. \tag{53}$$

The joint distribution (Eq. (30)) for multipoint measurements at times τ_j is

$$P^{(k+1)}(\tau_k x_k, \ldots, \tau_0 x_0) = \int \prod_{j=0}^{k} \frac{ds_j}{2\pi} \exp\left(-i \sum_{j=0}^{k} s_j x_j\right) \left\langle T \exp\left(\sum_j i s_j x(\tau_j)\right)\right\rangle. \tag{54}$$

The last factor in Eq. (54) may thus be obtained as a generating functional by taking

$$J(\tau) = -\sum_j s_j \delta(\tau - \tau_j), \tag{55}$$

where s_j is the Fourier variable conjugate to x_j.

We further introduce matrix notation along the trajectory for the two-point correlation functions:

$$\bar{M}_{jk} \equiv g_x^{(2)}(\tau_j - \tau_k).$$

Higher correlation functions may be computed using Eq. (53) yielding the factorized forms

$$\begin{aligned}
\langle x(\tau_j)x(\tau_l)\rangle &= \bar{M}_{jl},\\
\langle x(\tau_j)x(\tau_l)x(\tau_m)\rangle &= 0,\\
\langle x(\tau_j)x(\tau_l)x(\tau_m)x(\tau_n)\rangle &= \bar{M}_{jl}\bar{M}_{mn} + \bar{M}_{jm}\bar{M}_{ln} + \bar{M}_{jn}\bar{M}_{lm}.
\end{aligned} \tag{56}$$

These are typical for Gaussian fluctuations. Multipoint correlation functions are given by the sums of all possible pairings.

The joint probability distribution, Eq. (54), finally reads

$$\begin{aligned}
&P^{(k+1)}(\tau_k x_k, \ldots, \tau_0 x_0)\\
&= \int_{-\infty}^{\infty} \frac{\prod_j ds_j}{(2\pi)^{k+1}} \exp\left(-i\sum_j s_j x_j - \frac{1}{2}\sum_{jl}\bar{M}_{jl}s_j s_l\right)\\
&= \frac{1}{\sqrt{(2\pi)^{k+1}\det\bar{M}}} \exp\left(-\frac{1}{2}\sum_{jl}(\bar{M})^{-1}_{jl}x_j x_l\right).
\end{aligned} \tag{57}$$

Gaussian dynamics may or may not be Markovian. The Gaussian–Markovian case, known as the Uhlenbeck–Ornstein process, is obtained by choosing the overdamped oscillator spectral density setting $\gamma \gg \Omega$ in Eq. (48):

$$C(\omega) = \frac{1}{\mathcal{M}\Omega^2}\frac{\omega\Lambda}{\omega^2 + \Lambda^2}. \tag{58}$$

Using Eq. (52) this yields

$$g^{(2)}(t) = \frac{\mathbf{kT}}{\mathcal{M}\Omega^2}\exp(-\Lambda|t|). \tag{59}$$

The correlation matrix elements can now be factorized as $(\bar{M})_{ij} = M_i M_{i-1}\cdots M_{j+1}M_j$, where M_j depend on the time intervals between successive measurements, $M_j = \exp[(-\Lambda(\tau_{j+1} - \tau_j))]$. The inverse matrix is tridiagonal, and the joint distribution equation (57) is finally factorized into a product of Green's function:

$$P^{(k+1)}(\tau_k x_k, \ldots, \tau_0 x_0) = \rho(x_0)\prod_{j=0}^{k-1} G(\tau_{j+1}x_{j+1};\, \tau_j x_j), \tag{60}$$

where the Green function equation (42) and the equilibrium distribution equation (43) of the Fokker–Planck equation (41) are recovered.[49] The factorization (Eq. (60)) is a manifestation of the Markovian dynamics. It implies that ρ at a given time is sufficient to determine the future dynamics without the knowledge of the past history. The present derivation of Eq. (60) did not make any explicit assumption about Markovian property of the master equation.

Note however that Eq. (57) may not be generally recast in the form of Eq. (60). Memory effects show up for the spectral density other than Eq. (58). Gaussian processes with long algebraic tailed correlations were used to interpret some single-molecule experiments.[11,47]

When the oscillator spectral density can be represented by a sum of a few (K) terms of the type of Eq. (58) the dynamics is equivalent to that of K-uncorrelated overdamped harmonic degrees of freedom. The dynamics may be still considered Gaussian–Markovian, but in the higher K-dimensional space. This illustrates the point made previously. It might often be possible to develop a Markovian description by retaining a large number of degrees of freedom. However, if the only accessible observable is Q and the necessary number of degrees of freedom is too large, the Markovian description may not be very practical.

We shall apply the Gaussian model to calculate the joint probability of photon arrivals (Eq. (34)) for an arbitrary fluctuation timescale without invoking the slow fluctuation limit. Assuming small fluctuations, the decay rate is linear in the coordinate $\gamma = \bar{\gamma} + \gamma' Q$. We can

then express the PDF of arrival times exactly using the second-order cumulant expansion

$$P^{(k+1)}(\tau_k T_k, \ldots, \tau_0 T_0) = C_{k+1}^{-1} e^{-\sum_{l=0}^{k} \bar{\gamma} T_l} \times \exp\left[\frac{\gamma'^2}{2} \sum_{i,j=0}^{k} \int_0^{T_i} dt_i' \int_0^{T_j} dt_j' g_x^2(\tau_i + t_i' - \tau_j - t_j')\right].$$

For the Gaussian–Markovian process we substitute $g^{(2)} = \frac{\mathbf{kT}}{\mathcal{M}\Omega^2} e^{-\Lambda t}$ and get

$$P(\tau_k T_k, \ldots, \tau_0 T_0) = C_{k+1}^{-1} e^{-\sum_{l=0}^{k} \bar{\gamma} T_l} \times \exp\left[\frac{\mathbf{kT}\gamma'^2}{\mathcal{M}\Omega^2\Lambda^2}\left(\sum_{l=0}^{k}(\Lambda T_l + e^{-\Lambda T_l} - 1) + \sum_{ij,\tau_i>\tau_j}^{k} D(\tau_i, \tau_j, T_i, T_j)\right)\right].$$

For $T_j < |\tau_i - \tau_j|$, which implies that the excitation had decayed before the next laser pulse, we get

$$D(\tau_i, \tau_j, T_i, T_j) = e^{-\Lambda(\tau_i - \tau_j)}(1 - e^{-\Lambda T_i})(e^{\Lambda T_j} - 1).$$

Most generally, we have

$$D(\tau_i, \tau_j, T_i, T_j) = 2\Lambda(T_j + \tau_j - \tau_i) + e^{-\Lambda(\tau_i - \tau_j)}(1 - e^{-\Lambda T_i})(e^{\Lambda T_j} - 1) - 2\sinh\Lambda(\tau_j + T_j - \tau_i)$$

for $|\tau_i - \tau_j| < T_j < |\tau_i - \tau_j + T_i|$, and

$$D(\tau_i, \tau_j, T_i, T_j) = 2\Lambda T_i - e^{-\Lambda(T_j - \tau_i + \tau_j)}(e^{\Lambda T_i} - 1) - e^{-\Lambda(\tau_i - \tau_j)}(1 - e^{-\Lambda T_i})$$

when $T_j > |\tau_i - \tau_j + T_i|$. This limit should be avoided since photons from different pulses may not be distinguished in this case, which complicates the interpretation.

PDFs may be integrated numerically to get multipoint correlation functions. When $\gamma(Q)$ is not linear, the higher cumulants must be calculated.

The cumulant expansions and factorization equation (56) may be readily used to calculate the PAT correlation functions in slow limit. For instance, multipoint correlation function for ET quenching may be readily obtained by the second-order cumulant

$$g_T^{(1)} = k_{\mathrm{ET}}^{-1} \exp\left[\frac{3\mathbf{kT}\beta^2}{2\mathcal{M}\Omega^2}\right],$$

$$g_T^{(2)}(t_1) = k_{\mathrm{ET}}^{-2} \exp\left[\frac{3\mathbf{kT}\beta^2}{\mathcal{M}\Omega^2}\right] \exp[3\beta^2 g_x^{(2)}(t_1)],$$

$$g_T^{(3)}(t_2, t_1) = k_{\mathrm{ET}}^{-3} \exp\left[\frac{9\mathbf{kT}\beta^2}{2\mathcal{M}\Omega^2}\right] \exp[3\beta^2(g_x^{(2)}(t_1) + g_x^{(2)}(t_1 + t_2) + g_x^{(2)}(t_2))]. \quad (61)$$

Equation (61) may be directly applied to the Gaussian–Markovian process (Eq. (41)) by choosing $g_x^{(2)}$ according to Eq. (52). The second-order cumulant expansion may be similarly used to derive closed expressions for lineshapes and factorial moments for a two-level system modulated by Gaussian fluctuations either for stochastic or fully quantum Gaussian noise.[39]

We next illustrate the discussion of Eq. (36) and compare correlation functions of δT and $\delta\varphi$.

$$g_{\delta\varphi}^{(2)}(t_1) = \exp[\beta^2 g_x^{(2)}(0)]\left(\exp[\beta^2 g_x^{(2)}(t_1)] - 1\right), \quad (62)$$

$$g_{\delta T}^{(2)}(t_1) = \exp[3\beta^2 g_x^{(2)}(0)](\exp[3\beta^2 g_x^{(2)}(t_1)] - 2\exp[\beta^2 g_x^{(2)}(t_1)] + 1). \quad (63)$$

Leading δx^2 terms of Eqs. (62) and (63) coincide. For three-point functions

$$g^{(3)}_{\delta\varphi}(t_2,t_1) = \exp[(3/2)\beta^2 g_x^{(2)}(0)][\Theta - \exp[\beta^2 g_x^{(2)}(t_1)] - \exp[\beta^2 g_x^{(2)}(t_2)] - \exp[\beta^2 g_x^{(2)}(t_1+t_2)] + 2],$$

where

$$\Theta = \exp[\beta^2(g_x^{(2)}(t_1) + g_x^{(2)}(t_2) + g_x^{(2)}(t_1+t_2))], \quad \text{and}$$

$$\begin{aligned} g^{(3)}_{\delta T}(t_2,t_1) = \exp[(9/2)\beta^2 g_x^{(2)}(0)]\big[&\Theta^3 - \Theta(\exp 2\beta^2 g_x^{(2)}(t_1) \\ &+ \exp 2\beta^2 g_x^{(2)}(t_2) - \exp 2\beta^2 g_x^{(2)}(t_1+t_2)) \\ &+ \exp \beta^2 g_x^{(2)}(t_1) + \exp \beta^2 g_x^{(2)}(t_2) \\ &+ \exp \beta^2 g_x^{(2)}(t_1+t_2) - 1\big], \end{aligned}$$

however, δx^3 vanishes and the leading δx^4 terms differ significantly. Approximation equation (36) is thus not suitable for modeling higher (odd) moments.

3.3. *NonMarkovian dynamics: Renewal processes, continuous time random walks*

A nonMarkovian process is not fully characterized by its probability density at a given time; the history of the system does make a difference. In some cases reduced master equations for the system may be still derived. For example, a master equation which includes a time-convolution obtained using the Zwanzig projection operator technique[52] shows explicitly the memory functions and may be used for calculating two-point Green functions. However, it does not offer a prescription for calculating multipoint quantities. One cannot assume statistical independence of paths between points $x_0 \to x_1$ and $x_1 \to x_2$, and the resulting two-point PDFs may not generally be used to compute multipoint PDF using factorization into two-point Green function (Eq. (38)). The same is true for time-convolutionless master equations.[53]

In order to compute multipoint quantities one must introduce a more microscopic description of the process. The continuous time random walk (CTRW) provides an example of a solvable nonMarkovian model which nevertheless allows to compute multipoint quantities.[54] It generalizes ordinary random walks by introducing waiting time distribution functions (WTDF) for jumps. This model is suitable for modeling long-time memory effects.

We consider a particle moving stochastically on lattice points x (time is continuous, space is discrete). We define the transition probability W_{xy} for the jump from y to x

$$p(x; i+1) = \sum_y W_{xy} p(y; i), \tag{64}$$

where $p(x; i)$ is the probability to be at x after the ith jump and $\sum_x W_{xy} = 1$ ($W_{xx} = 0$ as jump necessarily implies change of position). This model represents a random walk.

The CTRW supplements this model by introducing the waiting time probability distribution for successive jumps, $\Psi_{xy}(t)$, normalized as $\int_0^\infty \Psi_{xy}(t)dt = W_{xy}$.

A fundamental property of the CTRW model is that the memory effects enter solely through the time elapsed from the last jump. At a given jump event the WTDF for the next jump Ψ is independent of the history. This *renewal* (resetting) property makes it possible to compute all statistical averages, even in the absence of a Markovian description for the probability distribution, and provides a convenient formalism for describing long-time memory effects.

To proceed, we introduce the matrix of survival probabilities $\Phi(t)$, that no jump had occurred prior to t. It is connected to the waiting time distribution by

$$\Phi_{xy}(t) = \delta_{xy} \int_t^\infty \sum_z \Psi_{zy}(t')dt'. \tag{65}$$

We denote the initial probability density to find the particle at x at time τ_0 by $\rho_x(\tau_0)$. The WTDF for the first jump after τ_0 ($\Psi'(t)$) may be different from $\Psi(t)$ since it depends on the past evolution of the system, including the time elapsed from the last jump. For long-tailed WTDF, the choice of $\Psi'(t)$ may substantially change the nature of the ensemble. Two important types of ensembles, which differ by the initial conditions, are commonly used.

(i) Assuming that all particles had arrived at their sites exactly at the initial time we simply set $\Psi'(t) = \Psi(t)$. This defines a nonstationary process and implies that specific preparation was made at the initial time. For models with short memory, this does not affect the long-time behavior. WTDFs with long algebraic tails where the CTRW may never be equilibrated are widely used to model subdiffusion and aging effects.[54] However, the lack of ergodicity makes it difficult to connect the calculated ensemble correlation functions with SMS experiments based on time averages.

(ii) Stationary processes require WTDF for the first jump

$$\Psi'_{xy}(t) = \int_t^\infty \Psi_{xy}(t')dt'/\bar{t}_y, \tag{66}$$

where $\bar{t}_y \equiv \int_0^\infty \tau \sum_x \Psi_{xy}(\tau)d\tau$ is the mean waiting time. Equation (66) is closely connected with microscopic reversibility, since it may be interpreted as connecting for first jump WTDF forward and backward (survival function).[55–57]

CTRW with infinite $\bar{t}$ does not represent a stationary random walk, since it asymptotically approaches a static sample and the mobility vanishes. A stationary CTRW is thus only possible if $\bar{t}$ is finite. This model does not require any special initial preparation; the initial time τ_0 is an arbitrarily chosen point in an ongoing random walk. This model is relevant for SMS since the time and ensemble averages are connected by the ergodic hypothesis. In addition we require the initial density ρ to be invariant to the jump event

$$\hat{W}\rho(\tau_0) = \rho(\tau_0). \tag{67}$$

Two simple models for $\hat{\Psi}$ are the discrete two-state jump model

$$\hat{\Psi} = \begin{pmatrix} 0 & \psi_d \\ \psi_u & 0 \end{pmatrix}$$

and the continuous variable dynamics describing diffusion in a harmonic potential[48]

$$\hat{\Psi} = \psi(t)\left(1 + D\bar{t}\left[\frac{\partial^2}{\partial x^2} + \frac{\partial}{\partial x}\frac{M\Omega^2 x}{\mathbf{kT}}\right]\right), \tag{68}$$

where D is the generalized diffusion constant.

The evolution of the density may be described by a master equation with fractional time derivatives.[58] However, the probability densities do not provide a full description of the system dynamics. Even though the (time-dependent) ratio connecting the density with jump rate can be defined,[59] the tendency to jump varies among various past trajectories, depending on the time elapsed from the last jump, and such rates cannot be used to compute multipoint correlation functions, as is done for Markovian processes. Instead, the density of arrival times plays a fundamental role in the theory. The total densities are finally obtained by convoluting the arrival densities with the survival function $\hat{\Phi}$.

We have developed a diagrammatic Green function method for calculating multipoint functions for this model. The stochastic path should be divided into segments between the first (at $\tau_{k-1} + \zeta_{2k-1}$) and the last ($\tau_k - \zeta_{2k}$) jump (renewal) in each interval t_k and connecting segments. Since some intervals contain no jump, they should be represented separately, and the complete k-point PDF consists of 2^k contributions which are represented by the diagrams shown in

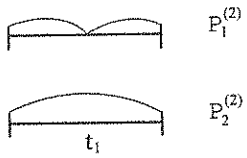

Fig. 4. Two contributions to the two-point PDF. Each diagram represents a path with (line meets the axis) or without (line does not meet the axis) some jump in each time interval.

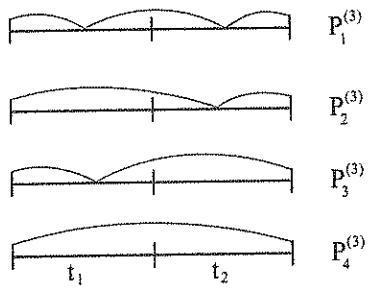

Fig. 5. The four contributions to the three-point PDFs.

Figs. 4–6. The presence of any (≥ 1) jump in a given time interval is depicted by a trajectory that touches the time axis. The probability $\Sigma_{xy}(t_k - \zeta_{2k-1} - \zeta_{2k})$ for jumping at $\tau_{k-1} + \zeta_{2k-1}$ to x if the path arrived at $\tau_k - \zeta_{2k}$ to y is given by solving the integral equation

$$\hat{\Sigma}(\tau) = \int_0^t \hat{\Psi}(\tau - \tau')\hat{\Sigma}(\tau')d\tau'; \quad \Sigma_{xy}(0) = \delta(\tau)\delta_{xy}. \tag{69}$$

This factor must be multiplied with probability for the connecting segments (between t_l and t_m interval), including the information about the x_j value carried by the trajectory at the boundary point τ_s projecting to the x_k at the interval boundaries τ, which is simply $\Psi(\tau_{l-1} - \tau_m + \zeta_{2l-1} + \zeta_{2m})|x_m\rangle\langle x_m|\delta_{l-1,l-2}\cdots\delta_{m+1,m})$. Similar factors must be included for the first and last segments with $\Psi \to \Psi', \Phi$.

Finally, we must integrate over all possible values of ζ, which are compatible with a diagram, e.g., for the first contribution to the

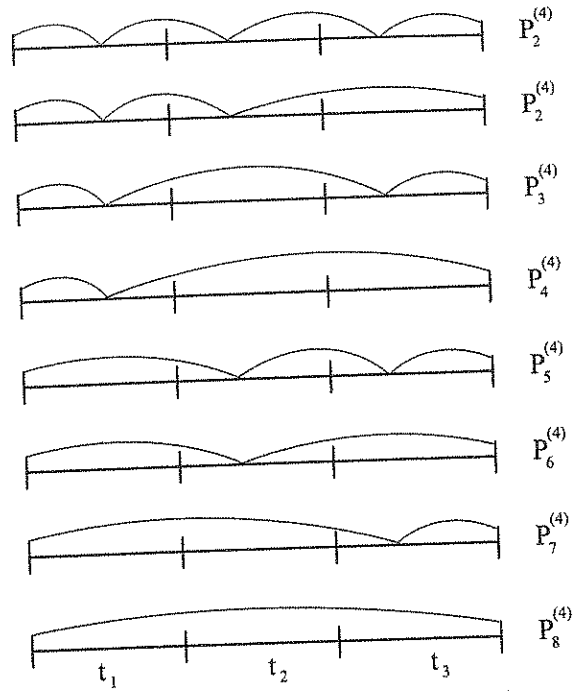

Fig. 6. The eight contributions to the four-point PDFs.

two-interval PDF, $P_1^{(3)}$

$$\begin{aligned} P_1^{(3)}(t_2 + t_1 x_2, t_1 x_1, 0 x_0) &= \int_0^{t_2} d\zeta_4 \int_0^{t_2-\zeta_4} d\zeta_3 \int_0^{t_1} d\zeta_2 \int_0^{t_1-\zeta_2} d\zeta_1 \\ &\times \langle x_2|\hat{\Phi}(\zeta_4)\hat{\Sigma}(t_2 - \zeta_4 - \zeta_3)\hat{\Psi}(\zeta_3 + \zeta_2)|x_1\rangle \\ &\times \langle x_1|\hat{\Sigma}(t_1 - \zeta_2 - \zeta_1)\hat{\Psi}'(\zeta_1)|x_0\rangle. \end{aligned} \tag{70}$$

These equations may be conveniently solved in Laplace space by defining $\hat{\Psi}(s) \equiv \int_0^\infty e^{-st}\hat{\Psi}(t)dt$, where s_k is the conjugate variable to the interval time t_k. Equation (69) is solved by $\Sigma(s) = [1 - \hat{\Psi}(s)]^{-1}$, and Eq. (70) is solved by the convolution theorem. Formal derivation of this algorithm may be found in Ref. 10. In the rest of this section

Table 1. Two contributions to the two-point PDF. Each column corresponds to one diagram of Fig. 4. + means interval with and − without a jump.

	$P_1^{(2)}$	$P_2^{(2)}$
t_1	+	−

we thus switch to Laplace space and set $P^{(k+1)}(s_k x_k, \ldots, s_1 x_1, x_0) = \int_{\tau_{k-1}}^{\infty} d\tau_k e^{s_k(\tau_k-\tau_{k-1}} \ldots \int_0^{\infty} d\tau_1 e^{s_1(\tau_1-\tau_0)} P^{(k+1)}(\tau_k x_k, \ldots, \tau_1 x_1, \tau_0 x_0)$

The two diagrams in Fig. 4 (Table 1) represent the contribution to the two-point PDFs, which are given by

$$P^{(2)}(s_1 x_1, x_0) = \sum_{j=1}^{2} P_j^{(2)} \rho_{x_0}(\tau_0), \tag{71}$$

$$P_1^{(2)} = \langle x_1 | \hat{\Phi}(s_1)[1 - \hat{\Psi}(s_1)]^{-1} \hat{\Psi}'(s_1) | x_0 \rangle,$$

$$P_2^{(2)} = \langle x_1 | \hat{\Phi}'(s_1) | x_0 \rangle.$$

The four diagrams in Fig. 5 (Table 2) represent the contribution to the three-point PDFs, which are given by

$$P^{(3)}(s_2 x_2, s_1 x_1, x_0) = \sum_{j=1}^{4} P_j^{(3)} \rho_{x_0}(\tau_0) \tag{72}$$

$$P_1^{(3)} = \left\langle x_2 \left| \hat{\Phi}(s_2)[1 - \hat{\Psi}(s_2)]^{-1} \frac{(\hat{\Psi}(s_2) - \hat{\Psi}(s_1))}{s_1 - s_2} \right| x_1 \right\rangle \times \langle x_1 | [1 - \hat{\Psi}(s_1)]^{-1} \hat{\Psi}'(s_1) | x_0 \rangle$$

$$P_2^{(3)} = \left\langle x_2 \left| \hat{\Phi}(s_2)[1 - \hat{\Psi}(s_2)]^{-1} \frac{(\hat{\Psi}'(s_1) - \hat{\Psi}'(s_2))}{s_2 - s_1} \right| x_1 \right\rangle \langle x_1 | x_0 \rangle$$

$$P_3^{(3)} = \left\langle x_2 \left| \frac{(\hat{\Phi}(s_2) - \hat{\Phi}(s_1))}{s_1 - s_2} \right| x_1 \right\rangle \langle x_1 | [1 - \hat{\Psi}(s_1)]^{-1} \hat{\Psi}'(s_1) | x_0 \rangle$$

Table 2. The four contributions to the three-point PDF corresponding to Fig. 5.

	$P_1^{(3)}$	$P_2^{(3)}$	$P_3^{(3)}$	$P_4^{(3)}$
t_2	+	+	−	−
t_1	+	−	+	−

$$P_4^{(3)} = \left\langle x_2 \left| \frac{(\hat{\Phi}'(s_2) - \hat{\Phi}'(s_1))}{s_1 - s_2} \right| x_1 \right\rangle \langle x_1 | x_0 \rangle.$$

Higher order correlation functions are constructed in a similar manner. Figure 6 (Table 3) shows eight diagrams representing all contributions to the four-point PDFs.

We shall demonstrate how Eqs. (71) and (72) work for the simplest PDFs: symmetric two-state ($\psi_u = \psi_d = \psi$, $\Phi_{xy} = \delta_{xy}\phi(t)$) with states $|-a_0\rangle$ and $|a_0\rangle$ undergoing CTRW from equilibrium $\rho_{a_0}(t_0) = \rho_{-a_0}(t_0) = 1/2$. The two-point PDF becomes

$$P^{(2)}(s_1 a_0, a_0) = P^{(2)}(s_1(-a_0), -a_0) = \frac{1}{2s_1} - \frac{\psi'(s_1)}{2s_1(1 + \psi(s_1))},$$

$$P^{(2)}(s a_0, -a_0) = P^{(2)}(s_1(-a_0), a_0) = \frac{\psi'(s_1)}{2s_1(1 + \psi(s_1))},$$

Table 3. The eight contributions to the four-point PDF corresponding to Fig. 6.

	$P_1^{(4)}$	$P_2^{(4)}$	$P_3^{(4)}$	$P_4^{(4)}$	$P_5^{(4)}$	$P_6^{(4)}$	$P_7^{(4)}$	$P_8^{(4)}$
t_3	+	+	+	+	−	−	−	−
t_2	+	+	−	−	+	+	−	−
t_1	+	−	+	−	+	−	+	−

and the two-point PAT correlation function is

$$g_T^{(2))}(t_1) = \frac{\varphi_u^4 + \varphi_d^4 - (\varphi_u^2 - \varphi_d^2)^2 \int_{-i\infty}^{i\infty} ds_1 e^{s_1 t_1} \frac{\psi'(s_1)}{s_1(1+\psi(s_1))}}{\varphi_u^2 + \varphi_d^2 - (\varphi_u - \varphi_d)^2 \int_{-i\infty}^{i\infty} ds_1 e^{s_1 t_1} \frac{\psi'(s_1)}{s_1(1+\psi(s_1))}}.$$

For the three-point PDF we obtain

$$\begin{aligned}
&P^{(3)}(s_2 x_2, s_1 x_1, x_0) \\
&= \frac{1}{(s_1 - s_2)} \frac{\phi(s_2)\psi'(s_1)(\psi(s_2) - \psi(s_1))}{(1 - \psi^2(s_1))(1 - \psi^2(s_2))} \\
&\quad \times \Big[\psi(s_1)\psi(s_2)(\delta_{a_0 x_0}\delta_{a_0 x_1}\delta_{a_0 x_2} + \delta_{-a_0 x_0}\delta_{-a_0 x_1}\delta_{-a_0 x_2}) \\
&\qquad + \psi(s_1)(\delta_{a_0 x_0}\delta_{a_0 x_1}\delta_{-a_0 x_2} + \delta_{-a_0 x_0}\delta_{-a_0 x_1}\delta_{a_0 x_2}) \\
&\qquad + \psi(s_2)(\delta_{-a_0 x_0}\delta_{a_0 x_1}\delta_{a_0 x_2} + \delta_{a_0 x_0}\delta_{-a_0 x_1}\delta_{-a_0 x_2}) \\
&\qquad + (\delta_{-a_0 x_0}\delta_{a_0 x_1}\delta_{-a_0 x_2} + \delta_{a_0 x_0}\delta_{-a_0 x_1}\delta_{a_0 x_2})\Big] \\
&\quad + \frac{1}{s_1 - s_2} \frac{(\psi'(s_2) - \psi'(s_1))\phi(s_2)}{1 - \psi^2(s_2)} \\
&\quad \times \Big[\psi(s_2)(\delta_{a_0 x_0}\delta_{a_0 x_1}\delta_{a_0 x_2} + \delta_{-a_0 x_0}\delta_{-a_0 x_1}\delta_{-a_0 x_2}) \\
&\qquad + (\delta_{a_0 x_0}\delta_{a_0 x_1}\delta_{-a_0 x_2} + \delta_{-a_0 x_0}\delta_{-a_0 x_1}\delta_{a_0 x_2})\Big] \\
&\quad + \frac{1}{(s_1 - s_2)} \frac{\psi'(s_1)(\phi(s_2) - \phi(s_1))}{1 - \psi^2(s_1)} \\
&\quad \times \Big[\psi(s_1)(\delta_{a_0 x_0}\delta_{a_0 x_1}\delta_{a_0 x_2} + \delta_{-a_0 x_0}\delta_{-a_0 x_1}\delta_{-a_0 x_2}) \\
&\qquad + (\delta_{-a_0 x_0}\delta_{a_0 x_1}\delta_{a_0 x_2} + \delta_{a_0 x_0}\delta_{-a_0 x_1}\delta_{-a_0 x_2})\Big] \\
&\quad + \frac{\phi'(s_2) - \phi'(s_1)}{s_1 - s_2}\left(\delta_{a_0 x_0}\delta_{a_0 x_1}\delta_{a_0 x_2} + \delta_{-a_0 x_0}\delta_{-a_0 x_1}\delta_{-a_0 x_2}\right).
\end{aligned} \tag{73}$$

Beyond the slow limit PAT statistics can be calculated by a modification of the present algorithm as described in Refs. 55, 56, and 60, where the same path integral as Eq. (34) was calculated for nonlinear spectroscopies.

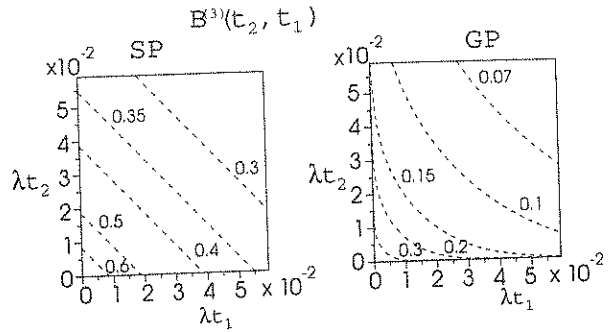

Fig. 7. Left: Contour plot for the three-point correlation function $\langle \delta \exp[\beta Q(\tau_2)] \delta \exp[\beta Q(\tau_1)] \delta \exp[\beta Q(\tau_0)] \rangle$, where $\delta \exp \beta \equiv \exp[\beta Q] - \langle \exp[\beta Q] \rangle$ for a stationary CTRW in a harmonic potential with WTDF (Laplace space) $\psi(s) = \frac{1+(\kappa\lambda)^\alpha}{1+(\kappa(s+\lambda))^\alpha}$ with $\alpha = 0.8$, $\frac{\lambda \mathbf{kT}}{DM\Omega^2} = 10^{-5}$, $(\beta\Omega^2/\mathbf{kT})^2 = 0.372$. Right: The same plot for Gaussian model with two-point correlation function identical to the left panel. Adapted from Ref. 10.

We next discuss the application of the CTRW models to slow dynamics and point out the differences from Gaussian fluctuations with the same algebraic long-tail correlation functions. In CTRW with algebraic WTDF tails a substantial fraction of particles remains for a long time at the same position (no jump). These fractions are responsible for the long tails of the correlation functions. Based on this picture, we may draw some conclusions. In Fig. 7, we display the three-point correlation function $B^{(3)}$ of $\delta \exp(\beta x)$ (which corresponds to ET quenching correlation function) for a CTRW in a harmonic potential[10] Eq. 68 with algebraic tails $\psi(t) \sim t^{\alpha-1} e^{-\lambda t}$. λ is introduced as a cutoff parameter to represent a stationary ensemble (SP) with a finite $\bar{t}$. Three-point correlation plots are also shown for the Gaussian model with the same two-point correlation function. The linear contours of the CTRW model suggest that correlations depend on the total time $t_1 + t_2$, and not on $t_1 - t_2$ alone. It reflects the dominant asymptotic contribution of particles which survive the entire history and stay near the starting point. Gaussian dynamics shows more curved contours which depend on both t_1 and t_2 in a more complex way.

We see substantial differences between the asymptotic behavior of the two models. We further recast these observations into a simple analytic argument. We shall consider Gaussian and CTRW processes with power law two point correlation $g_x^{(2)} \sim t^{-\alpha}$; for CTRW see Appendix B of Ref. 10 for the construction of the model. We shall compare the four-point correlation function $g_x^{(4)} = \langle x(3t)x(2t)x(t)x(0)\rangle$ at long times for both models. For the Gaussian model $g^{(4)} \sim [g_x^{(2)}(t)]^2 + [g_x^{(2)}(2t)]^2 + g_x^{(2)}(3t)g_x^{(2)}(t)$, i.e. for power law $g^{(2)}(t) \sim t^{-\alpha}$ it gives $g^{(4)} \sim t^{-2\alpha}$ while CTRW is asymptotically given by fraction of long-surviving particles and so $g^{(4)}(t) \sim g^{(2)}(t) \sim t^{-\alpha}$.

4. Summary

We have introduced factorial moments of photon statistics and related them to the multipoint correlation functions. We have also given the weak field perturbation theory of photon counting and drew the connection to nonlinear spectroscopies, recasting them in terms of the same multipoint correlation functions of dipole moments. We have shown two limits of single-molecule experiments, where the correlation function of observed quantities may be related to the correlation functions of classical stochastic coordinate. We have discussed three examples of nonequivalent solvable stochastic models which are particularly suitable for phenomenological modeling of single experiments.

Acknowledgments

The authors acknowledge the support of the National Science Foundation (Grant CHE-0745892) and NIRT (Grant EEC-0303389) and the National Institutes of Health (Grant GM 59230). F. Š. acknowledges the support of the Ministry of Education, Youth and Sports of the Czech Republic (project MSM 0021620835) and the Grant Agency of the Czech Republic (Grant. No. 202/07/P245).

References

1. W. E. Moerner and L. Kador, *Physical Review Letters* **62** (1989) 2535.
2. M. Orrit and J. Bernard, *Physical Review Letters* **65** (1990) 2716.
3. F. Kulzer and M. Orrit, *Annual Reviews Physical Chemistry* **55** (2004) 585.
4. I. S. Osad'ko, *Selective Spectroscopy of Single Molecules*, Springer Series in Chemical Physics, Vol. 69 (Springer, Berlin, 2002).
5. C. W. Gardiner and P. Zoller, *Quantum Noise: A Handbook of Markovian and Non-Markovian Quantum Stochastic Methods with Applications to Quantum Optics* (Springer, 2004).
6. S. C. Kou, X. S. Xie and J. S. Liu, *Applied Statistics* **54** (2005) 469.
7. V. Barsegov and S. Mukamel, *Journal of Physical Chemistry* **108** (2004) 15.
8. V. Barsegov and S. Mukamel, *Journal of Chemistry Physics* **117** (2002) 9465.
9. V. Barsegov, V. Chernyak and S. Mukamel, *Journal of Chemical Physics* **116** (2002) 4240.
10. F. Šanda and S. Mukamel, *Physical Review E* **72** (2005) 031108.
11. S. C. Kou and X. S. Xie, *Physical Review Letters* **93** (2004) 180603.
12. X. Brokmann, J.-P. Hermier, G. Messin, P. Desbiolles, J.-P. Bouchaud and M. Dahan, *Physical Review Letters* **90** (2003) 120601.
13. O. Flomenbom, K. Velonia, D. Loos, S. Masuo, M. Cotlet, Y. Engelborghs, J. Hofkens, A. E. Rowan, R. J. M. Nolte, F. C. de Schryver and J. Klafter, *Proceedings of the National Academy of Sciences* (USA) **102** (2005) 2368.
14. S. Mukamel, *Principles of Nonlinear Optical Spectroscopy* (Oxford University Press, New York, 1995).
15. M. Kuno, D. P. Fromm, H. F. Hamman, A. Gallagher and D. J. Nesbitt, *Journal of Chemical Physics* **112** (2000) 3117.
16. K. T. Shimizu, R. G. Neuhauser, C. A. Leatherdale, S. A. Empedocles, W. K. Woo and M. G. Bawendi, *Physical Review B* **63** (2001) 205316.
17. Y. Jung, E. Barkai and R. Silbey, *Chemical Physics* **284** (2002) 181.
18. G. Margolin, V. Protasenko, M. Kuno and E. Barkai, *Journal of Physical Chemistry B* **110** (2006) 19053.
19. Y. He and E. Barkai, *Physical Review Letters* **93** (2004) 068302.
20. F. Šanda and S. Mukamel, *Journal of Chemical Physics* **125** (2006) 014507.
21. G. Lindblad, *Communications in Mathematical Physics* **48** (1976) 199.
22. G. S. Agarwal, in *Springer Tracts in Modern Physics* 70, ed. G. Höhler (Springer, New York, 1974).
23. R. H. Dicke, *Physical Review* **93** (1954) 99.
24. J. von Neumann, *Mathematical Foundations of Quantum Theory* (Princeton University Press, 1955).
25. G. Bel and E. Barkai, *Physical Review Letters* **94** (2005) 240602.
26. G. Margolin and E. Barkai, *Physical Review Letters* **94** (2005) 080601.
27. D. E. Makarov and H. Metiu, *Journal of Chemical Physics* **115** (2001) 5989.

28. S. A. Rice and M. Zhao, *Optimal Control of Molecular Dynamics* (Willey, New York, 2000).
29. E. Barkai, Y. Jung and R. Silbey, *Annual Reviews of Physical Chemistry* **55** (2004) 457.
30. S. Mukamel, *Physical Review A* **68** (2003) 063821.
31. R. Zwanzig, *Nonequilibrium Statistical Mechanics* (Oxford University Press, New York, 2001).
32. G. C. Hegerfeldt, *Physical Review A* **47** (1993) 449.
33. R. J. Cook, *Physical Review A* **23** (1981) 1243.
34. D. Lenstra, *Physical Review A* **26** (1982) 3369.
35. R. J. Glauber, in *Quantum Optics and Electronics*, eds. C. DeWitt, A. Blandin and C. Cohen-Tannoudji (Gordon and Breach, New York, 1964).
36. Y. Zheng and F. L. H. Brown, *Journal of Chemical Physics* **119** (2003) 11814.
37. T. Basché, W. E. Moerner, M. Orrit and H. Talon, *Physical Review Letters* **69** (1992) 1516.
38. Y. Zheng and F. L. H. Brown, *Journal of Chemical Physics* **121** (2004) 7914.
39. F. Šanda and S. Mukamel, *Physical Review A* **71** (2005) 033807.
40. Y. Jung, E. Barkai and R. Silbey, *Advances in Chemical Physics* **123** (2002) 199.
41. E. Barkai, Y. Jung and R. Silbey, *Physical Review Letters* **87** (2001) 207403.
42. Y. Tanimura, *Journal of the Physical Society of Japan* **75** (2006) 082001.
43. U. Harbola, J. B. Maddox and S. Mukamel, *Physical Review B* **73** (2006) 075211.
44. H. Yang, G. Luo, P. Karnchanaphanurach, T.-M. Louie, I. Rech, S. Cova, L. Xun and X. S. Xie, *Science* **302** (2003) 262.
45. V. Barsegov and S. Mukamel, *Journal of Chemical Physics* **116** (2002) 9802.
46. T. Förster, in *Modern Quantum Chemistry, Part III: Action of Light and Organic Molecules*, ed. O. Sinanoglu (Academic, NewYork, 1965), p. 63.
47. W. Min, G. Luo, B. J. Cherayil, S. C. Kou and X. S. Xie, *Physical Review Letters* **94** (2005) 198302.
48. H. Risken, *The Fokker-Plank Equation* (Springer, Berlin, 1989).
49. V. Chernyak, F. Šanda and S. Mukamel, *Physical Review E* **73** (2006) 036119.
50. A. O. Caldeira and A. J. Leggett, *Physical A* **121** (1983) 587.
51. T. l. C. Jansen and S. Mukamel, *Journal of Chemical Physics* **119** (2003) 7979.
52. R. Zwanzig, *Lectures in Theoretical Physics (Boulder)* **3** (1960) 106.
53. N. Hashitsume, F. Shibata and M. Shingu, *Journal of Statistical Physics* **17** (1977) 155.
54. J. Klafter, M. F. Shlesinger and G. Zumofen, *Physics Today* **49** (1996) 33.
55. F. Šanda and S. Mukamel, *Physical Review E* **73** (2006) 011103.
56. F. Šanda and S. Mukamel, *J. Chem. Phys.* **127** (2007) 154107.
57. H. Qian and H. Wang, *Europhysical Letters* **76** (2006) 15.

58. R. Metzler and J. Klafter, *Physics Reports* **339** (2000) 1.
59. F. Barbi, M. Bologna and P. Grigolini, *Physical Review Letters* **95** (2005) 220601.
60. F. Šanda and S. Mukamel, *Physical Review Letters* **98** (2007) 080603.
61. V. Chernyak and S. Mukamel, *J. Chem. Phys.* **105** (1996) 4565.